Multi-omics analysis reveals a non-canonical regulatory pattern of UPL3 on carbon metabolism related cell senescence

Wei Lan, Weibo Ma, Shuai Zheng, Yuhao Qiu, Haisen Lu, Chenxing Huang, Yu Zhang, Ying Miao (ymiao@fafu.edu.cn)

Fujian Provincial Key Laboratory of Plant Functional Biology, College of Life Sciences, Fujian Agriculture and Forestry University https://orcid.org/0000-0003-2220-455X

Research Article

Keywords: HECT-type ubiquitin ligase, Amino acid metabolism, Carbon fixation, DUBs, Senescence

Posted Date: January 26th, 2022

DOI: https://doi.org/10.21203/rs.3.rs-1264931/v1

Abstract

The HECT domain-containing UPL3 ligase plays critical roles in plant development and stress protection, but its mechanism of action remains limited. To globally identify its targets in *Arabidopsis thaliana*, we conducted proteomic analyses of ubiquitinated proteins in *upl3* mutants *via* label-free mass spectrometry. In 6-week-old plants, a landscape of UPL3-dependent ubiquitinated proteins is constructed based on correlated datasets of ubiquitome, proteome, and transcriptome. Preferential ubiquitination of proteins related to carbon fixation represented the largest set of proteins with increased ubiquitination in the *upl3* plant, while a small set of proteins with reduced ubiquitination caused by the *upl3* mutation were linked to cysteine/methionine synthesis and protein translation processes. Furthermore, the *upl3* mutation led to an increase in ubiquitination of some of proteins including chromatin remodeling ATPase (BRM), histone proteins, and most of carbon metabolic enzymes, but decreased the ubiquitination of hexokinase 1 (HXK1), phosphoenolpyruvate carboxylase 2 (PPC2), ribosomal protein S5, and H1/H5 domain proteins. Notably, ubiquitin hydrolase 12 (UBP12), BRM, and PPC2 were identified as the UPL3-interacting partners by both GFP-nanotrap-Mass-Spectrometry analyses and yeast two-hybrid assay. Characterization of *upl3*, *brm*, and *ubp12* mutant plants and transcriptome analysis suggested that UPL3 fine-tunes carbon metabolism mediating cellular senescence by interacting with UBP12, BRM, and PPC2 in the nucleus. Our results highlight an important function of UPL3 as a hub of regulator on proteolysis-independent regulation and proteolysis-dependent degradation.

Introduction

Cell senescence, including developmental senescence and stress induced cell senescence, is triggered by internal and external factors, and often involves degradation and remobilization of cellular components. During plant senescence, a visible change of leaf yellowing is an indication of chloroplast damage and chlorophyll degradation. At the molecular level, catabolism of macromolecules is a major event in senescent cells, especially involving proteolysis. It has been documented that during *Arabidopsis* leaf senescence, alterations in transcriptional regulation, histone-associated epigenetic processes, posttranslational modification, and macromolecule/organelle degradation are genetically determined and developmentally programmed (Buchanan-Wollaston, 2005; Woodson, 2015; Yolcu, 2017). Pathways for protein degradation include the 26S proteasome, a protein complex involved in the degradation of polyubiquitinated substrates, the organelle degradation, autophagy processes, and the monoubiquitination- or short ubiquitin-chain-dependent proteinases (Vierstra, 2009; Berndsen and Wolberger, 2014; Lan and Miao, 2019). The targeting for 26S proteasome degradation is a sequential process that starts with the ubiquitin activation by the E1 (ubiquitin-activating) enzyme in an ATP-dependent manner. The activated ubiquitin is then transferred from the E1 to the E2 (ubiquitin-conjugating) enzyme that acts as an intermediate. Finally, the E3 (ubiquitin ligase) enzyme mediates the deposition of the activated ubiquitin to, normally, a lysine residue of the target protein. Depending on the E3 type, protein ubiquitination may be a direct or indirect process (Berndsen and Wolberger, 2014; Zheng et al., 2017).

The HECT E3 ligase family contains seven members (UPL1-UPL7) in *Arabidopsis*, which play important roles in protein fate and protein function during the senescence process (Lan and Miao, 2019). Although animal studies have revealed diverse mechanisms in the functions and regulation of HECT E3s, their plant counterparts are less explored. So far, the *Arabidopsis* UPL3 and UPL5 are known to be involved in plant development and response to stress (Bensussan et al., 2015; Downes et al., 2003; Furniss et al., 2018; Miao and Zentgraf, 2010; Miller et al., 2019; Patra et al., 2013). While the *upl5* mutant shows a premature aging phenotype, UPL3 functions in trichome, vascular and seed development, as well as in immune response. The UPL5 protein is able to target the transcription factor WRKY53 for ubiquitination and degradation, playing an antagonist role in leaf senescence (Miao et al., 2004; Miao and Zentgraf, 2010). UPL3 may target GLABROUS 3 (GL3) and ENHANCER OF GL3 (EGL3), two bHLH transcription factors, and positively regulate trichome development and flavonoid biosynthesis in *Arabidopsis* (Patra et al., 2013). The *upl3* mutant shows larger stem diameter than that of the WT plant, indicating a role of UPL3 in regulation of vascular development (Bensussan et al., 2015). UPL3 was also demonstrated to promote proteasomal processivity that is required for development of plant immunity (Furniss et al., 2018). Recently, Miller et al. showed that UPL3 controls the protein stability of LEAFY COTYLEDON2 (LEC2), a key transcriptional regulator of seed maturation, and regulates the seed size and crop yields (Miller et al., 2019). Thus, UPL3 emerges as a critical player with multiple roles in *Arabidopsis thaliana*, probably acting as a regulatory hub for a number of signaling pathways. However, the underlying mechanisms are still limited understood.

In this study, we conducted globally proteomic and ubiquitomic analyses by using a label-free mass spectrometry-based analysis of protein ubiquitination using K-epsilon-GG remnant antibody enrichment approach in the *upl3* mutant relative to wild-type to construct a landscape of UPL3-dependent ubiquitylated proteins, and analysis of ubiquitin footprint provide direct evidence of the ubiquitination of proposed target proteins. GFP-nanotrap mass spectrometry and yeast two hybrid assay further confirmed direct UPL3 target proteins. Further UPL3-interacting proteins combined with their mutant's phenotyping and analysis of transcriptome dataset suggested that UPL3 targeted deubiquitination enzymes (DUBs) and acted as regulators that activate or repress the UPL3 activity, impacting on carbon-metabolism-related proteins and metabolism related cell senescence.

Results

Mutation of UPL3 affects plant development

In order to address more defined roles of UPL3, we systematically analyze the phenotype of *upl3* lines, two knockout lines (*upl3-1*, *upl3-3*), two overexpressing lines (*oeUPL3-24*, *oeUPL3-39*), and two complementation lines (*comUPL3-1, comUPL3-2*) were produced and confirmed at the transcriptional and protein levels (Figure1A-B; Supplementary Figure S1). The predicted size of the entire protein is ~250 kDa appeared in *oeUPL3-24/-39* lines, along with an additional 100 kDa band (possible alternative splicing isoform or proteolysis statue) is yet to be confirmed by sequencing. Plants of the *upl3* lines exhibited apparently downward-curled leaves and a two-week delay in bolting and leaf senescence, compared to

the wildtype (WT) plant (Figure 1C, G, H). In contrast, the overexpressing UPL3 lines displayed premature leaf aging and one-week earlier bolting (Figure 1C, G, H). Complementation by the full-length UPL3 rescued the *upl3* mutants' phenotypes (Figure 1C). Consistently, chlorophyll content (Figure 1D), photosystem II fluorescent activity (Fv/Fm) (Figure 1E) and green leaves/yellow leaves ratio (Figure 1F) increased significantly in the *upl3* lines and decreased in the *oeUPL3* line, compared to the WT. Thus, UPL3 functions in organ development and aging by accelerating cell senescence, under natural developmental conditions.

Loss of UPL3 induces global ubiquitin enrichment in 6-week-old upl3 **plants**

UPL3 was highly expressed in senescent leaf (after 6 weeks) (Winter et al., 2007; Supplementary Fig. S2), therefore, we performed a label-free mass spectrometry (MS)-based analysis of protein ubiquitination using K-epsilon-GG remnant antibody enrichment approach using 6-week-old *upl3* and WT plants (Figure 2A; Supplementary Fig. S3). Identified proteins based on their tandem mass spectra matching against the UniProt *Arabidopsis thaliana* Columbia database (current total of 39211 reads) using the MaxQuant software, are listed in Supplementary Dataset 1. Label-free quantification (LFQ), with a false discovery rate (FDR) adjusted to < 1% and a minimum score for modified peptides set as > 40, resulted in a set of over 1,310 potential ubiquitinated targets. This was further refined to a subset of 1155 targets by at least two post-translational modifications (PTMs) (Figure 2B; Supplementary Data Set 2).

To identify the alteration of ubiquitin conjugates associated with the *upl3* mutation, a fold-change greater than 1.2 or less than 1/1.2 was used to filter conjugate targets in the library, whose ubiquitination was up-regulated or down-regulated. All the differentially ubiquitin conjugates (DUCs) data in *upl3*/WT were shown in Figure 2B and Supplementary dataset S2. Among them, ubiquitination of 545 sites (356 proteins) was found to be up-regulated, and ubiquitination of 198 sites (189 proteins) was down-regulated in the *upl3*, compared to WT plant (Figure 2B). These results were verified by global ubiquitination immunodetection using an anti-ubiquitin antibody, in which deletion of *UPL3* led to enhanced signals of global levels of protein ubiquitination, whereas loss of its homolog *UPL5* did not, as a control (Figure 2C, Miao and Zentgraf, 2010). Overexpression of *UPL3* retained comparable global levels of protein ubiquitination with the WT (Figure 2C). Indeed, more proteins were found in the up-regulated category than in the down-regulated set, in term of modified protein sites (Figure 2D). Specifically, 188 conjugates had enhanced abundance over WT by greater than 1.5-fold, while the levels of only 79 conjugates were reduced by 1/1.5 or less (Figure 2D). Fold-change levels against the statistic P value of individual ubiquitinated site were plotted to give more details on the dataset (Figure 2E). Of them was the fact that ubiquitin-conjugating enzyme 35 (UBC35) and ubiquitin-activating enzyme 1 (UBA1) were among the targets with significantly enhanced ubiquitination levels (Figure 2E), which appeared in the dataset of ubiquitome (Miller et al., 2010), and RPN, a known target of UPL3 (Furniss et al., 2018), was appeared in dataset of ubiquitome with upregulated ubiquitination level, indicating that the quality of ubiquitome dataset was properly sound. Together, this surprising rise in protein ubiquitination caused by loss of UPL3 perhaps means that UPL3 has somehow function on deubiquitinating pathway or UPL3 promotes deubiquitinases (DUBs) function.

Differential ubiquitomic enrichment reveals that metabolic enzymes are among the processes significantly affected by UPL3

GO term enrichment showed that the molecular functions of assembled ubiquitin conjugates were related to protein-protein interactions (47%), catalytic activity (34%), transport activity (7%), structural molecule activity (5%), and other (7%). However, for the differentially ubiquitin conjugates (DUCs) of *upl3* relative to WT, the protein-protein interaction function enrichment was increased to 49% (Figure 3A), implying a major involvement in molecular interaction for the UPL3-regulated targets. Further assignment to biological processes showed that the DUCs included mainly proteins involved in the response to metal ion stresses and enzymes related to carbon metabolism and nucleotide metabolism (Supplementary Figure S4). Hence, it is plausible that UPL3 maintains the ubiquitination status of enzymes and regulatory factors to fine-tune cellular metabolism.

This notion was further validated *via* KEGG pathway analysis (Figure 3B; Supplementary Fig S4). A large subset of the DUCs were enzymes related to biosynthesis of secondary metabolites, carbon fixation, carbon metabolism, and amino acid metabolism. The ubiquitinated forms of the Calvin-Benson enzymes, such as ribulose-1,5-P_2-carboxylase (RuBisCO), phosphoglycerate kinase (PGK), glyceraldehyde-3-phosphate dehydrogenase (GAPDH) and the aldoketo reductase family members (ALDOs), as well as the CAM enzymes malate dehydrogenases MDH1 and MAEB homolog, were enriched in the *upl3* plants (Figure 3C). Carbon metabolism was also represented by a reduction in ubiquitin conjugates of phosphoenolpyruvate carboxylase (PPC2) and hexokinase-1 (HXK1) in the *upl3* background. On the other hand, a decline in ubiquitin conjugates was found in a small subset of cysteine and methionine metabolism-related enzymes, such as 5-methyltetrahydropteroyl-triglutamate, homocysteine methyltransferase 2 (MS2), S-adenosylmethionine synthase 1 (SAM1), cysteine synthase 1 (OASA1), and methionine aminotransferase (BCAT4), SNARE-like superfamily protein (YKT61), vesicle-associated membrane protein 714 (VAMP714) in the *upl3* plants (Figure 3D, Supplementary Dataset S2).

Our *Arabidopsis* ubiquitome proteins can be classified as cytoplasmic (36%), nuclear (20%), chloroplast (20%), membrane (14%) and others (10%). Among these, the percent ratio of the UPL3-influenced ubiquitin conjugates was higher in the cytoplasmic and the nuclear sections (Figure 3E). According to fold-change categories of DUCs, most of the proteins in Q1, experiencing large drop in ubiquitination (0 < fold change < 1/1.5) were chloroplast and chromatin components; most of those in Q2 (1/1.5 < fold change < 1/1.2) were vacuole and endomembrane components. In contrast, most of the enriched ubiquitin conjugates in Q3 (1.2 < fold change < 1.5) were components of the stromal and vesicle membrane; and the proteins with the most significantly up-regulated ubiquitination, Q4 (fold change > 1.5) were predicted to be cytoplasmic (Supplementary Figure S5). The Cytoscape protein-protein interaction network of the 545 UPL3-influenced DUCs generated distinctly clustered interaction nodes (Supplementary Fig S6) (Shannon, 2003). The UPL3-influenced conjugates were dispersed throughout the network, suggesting that UPL3 was likely involved in broad control of stress response (Supplementary Fig S6A). The network also revealed a relatively significant enrichment in response to stimulation (abiotic or biotic) of the translation machinery and protein metabolism (Supplementary Fig S6B). However, UPL3

fused GFP transformed transiently in tobacco leaves showed that UPL3 was clearly localized in the nucleus (Figure 3F). Therefore, nuclear proteins such as those functioning in chromatin remodeling, chromosome regulation, and transcriptional complexes are likely primary UPL3-dependent targets.

The UPL3-dependent conjugates are enriched in histone H1/H5 and stress-related protein domains

Scanning protein domains of the DUCs using InterProScan identified several UPL3-dependent (reduced ubiquitination in the *upl3* background) protein domains including the histone H1/H5 domain, jacalin-like lectin domain, GST domain, S15/NS1 RNS binding domain, and heavy metal associated domain (Figure 4A blue), whilst the UPL3–influenced ubiquitin conjugates (enhanced ubiquitination in the *upl3* background) contained leucine-rich repeat, histone H2A/H2B/H3, ribosomal protein S5, double-stranded RNA binding domain, and histone fold domains (Figure 4A orange). For protein domains of the individual DUC within each fold-change range (Q1, Q2, Q3 and Q4), the results were shown in Supplementary Figure S4 and Supplementary dataset S2. Again, it was noted that protein domains associated with RNA binding, protein translation, and amino acid synthesis related proteins were overrepresented in proteins showing reduced ubiquitination in the *upl3* plants, followed by heavy-metal-associated domain, remorin- and jacalin-like lectin domain of abiotic (metal)/biotic stress responsive proteins. In contrast, protein domains associated with protein binding, transport ATPase, ubiquitin carboxyl-terminal hydrolase, and metabolism enzyme were the most significant domains in proteins showing enhanced ubiquitination in the *upl3* plants, followed by domains contained in the ubiquitination/26S proteasome system (UPS) regulatory complex (Supplementary Fig S4; Supplementary dataset S2). It suggested that proteins containing heavy-metal-associated domains, GST domains, jacalin-like lectin domains, and histone H1/H5 domains were likely UPL3-dependent ubiquitin conjugates. Consistently, UPL3–influenced ubiquitin conjugates contain histone H2A/H2B/H3, histone fold, and SPK1/BTB/POZ binding domain, most of which have functions related to protein binding activity and gene transcriptional control.

Histone ubiquitination was earlier recognized as a marker of transcriptionally active chromatin, where the ubiquitinated forms of histones H2B/H2A were associated specifically with activated or repressed transcribed genes (Cao et al., 2008; Kralemann et al., 2020). It was also reported that the H1 (or linker) histone played critical functions in determining the accessibility of chromatin DNA to trans-acting factors and mediated chromatin organization in the epigenetic control during developmental and cellular transitions (Kotinski et al., 2017; Rutowicz et al., 2019). In this scenario, UPL3–influenced ubiquitin conjugates in the nucleus are likely mediators of chromatin accessibility and transcriptional processes that control downstream gene expression. To test this hypothesis, we compared transcriptome data of the *upl3* and WT plants, which released from Furniss (2018) (Supplementary dataset S3). A total of 1467 differentially expressed genes between the *upl3* and WT seedlings were identified (Figure 4B; Supplementary Dataset S3). Of these, genes related to stress responses (drug, hypoxia, oxidative, and UV) were most significantly upregulated, followed by genes associated with cellular glucan metabolic processes, anthocyanin-containing compound biosynthesis, and cellular polysaccharide catabolic processes. A third set of up-regulated genes was involved in protein transport and leaf senescence. In contrast, genes for response to (a)biotic stress (metal ion salt stress, and fungus) and plant aging were

most significantly downregulated, followed by genes related to secondary metabolic processes, MAPK signaling pathway, leaf cell death, and phenylpropanoid biosynthesis (Figure 4C). Based on a delaying senescence phenotype of *upl3* mutant, we further selected 14 genes coding for transcription factors such as WRKYs, NACs, ZFs, and MYB related to leaf aging (e.g., WRKY53 and WRKY75; Miao and Zentgraf, 2007; Guo et al., 2017) and salicylic acid responsive senescence (e.g., WRKY38, WRKY63, and WRKY51 etc.; Zhang et al., 2017; Krinke et al., 2009) for confirmative RT-qPCR analysis (Figure 4D). The results showed that the expression level of *WRKY53, WRKY75, WRKY38, WRKY63 and WRKY51*, as well as *ZFs* was significantly decreased in the *upl3* (Figure 4D). These data confirmed the notion that UPL3 had a profound functional involvement in stress responsive cell senescence, developmental cell senescence (aging), and secondary metabolic processes, possibly *via* ubiquitination of their regulators either directly or indirectly.

Furthermore, 26 proteins were identified as the overlapping genes of DEGs and DUCs, with altered ubiquitinated protein level (fold-change > 1.5) and gene expression level (fold-change > 1.3) by the *upl3* mutation (Figure 4B). Among these proteins, four proteins (Figure 4E, fold-change depicted with two orange value) with increased ubiquitin conjugation were up-regulated in gene expression in the *upl3* background, including glucomannan 4-beta-mannosyltransferase 9 (CSLA9), inositol-3-phosphate synthase isozyme 1 (MIPS1), calcium-binding protein 16 (CML16), and the Patellin-2 (PATL2) (Figure 4E). Two other proteins (Figure 4E, fold-change depicted with a blue and an orange value) with reduced ubiquitin conjugates but with increased transcript level in the *upl3* mutant were cysteine lyase (CORI3) and cinnamyl alcohol dehydrogenase 7 (CAD7), both of which had reported functions in the amino acid metabolic process (Tsuwamoto and Harada, 2011; Tanaka et al., 2018). On the other hand, 9 proteins (Figure 4E, fold-change depicted with an orange and a blue value) showed an enhanced ubiquitin conjugation level but a down-regulated expression level in the *upl3* mutant plants. These included calmodulin-like protein10 (CML10), aquaporin (PIP1-5), triacylglycerol lipase-like 1 (TLL1), leucine-rich repeat ser/thr protein kinase (LRR-RLK), the jacalin-related lectin 23 (JAL23), ABCB transporter member 19 (ABCB19), methionine aminotransferase (BCAT4), and the ankyrin repeat-containing protein (BDA1), whose functions were involved in response to (a)biotic stress and in plant development and plant aging in response to light, auxin, JA, or calcium (Debernardi et al., 2014; Wu et al., 2010; Yang et al., 2012 ; Yang et al., 2013). The remaining eleven proteins (Figure 4E, fold-change depicted in blue) were those with both reduced ubiquitin conjugation level and down-regulated gene expression in the *upl3* mutant. Their functions seemed to be related to glycoside metabolism and transport pathways. From these data, it is obvious that the UPL3-centered molecular network involves both feed-forward and feed-back regulatory pathways and mostly impacts on cellular metabolism, stress responsive cell death and aging.

Identifying the potential ubiquitylated targets in UPL3-bound proteins

To evaluate the direct connection between UPL3 and conjugates, we assessed protein-protein interaction using a GFP-nanotrap-assisted pulldown-MS assay (Supplementary Figure S7), in which the GFP-tagged UPL3 was a bait. To do this, the rosette leaves of 6-week-old stable transgenic plants expressing either

the UPL3-GFP or the control GFP driven by the *ACTIN3* promoter were used for total protein isolation, purification and immunodetection (Figure 5A-B). The trypsin-digested proteins were subjected to mass spectrometry analysis with high-energy collisional dissociation quantum efficiency mass spectrometry (QE-MS). Tandem mass spectra were searched against UniProt *Arabidopsis thaliana* Columbia (89247_20181227) database *via* Mascot2.2 software. A total of 81 putative proteins were identified after subtracting the GFP control resulted from the UPL3-GFP candidate list (Supplementary Dataset S5). With these putative UPL3-interacting patterns, we identified 29 (or 11 under more stringent conditions) overlapping proteins in the ubiquitome DUCs (Figure 5C).

These 29 proteins were clustered in four categories based on the KEGG pathway database. Consistently, proteins involved in the carbon fixation pathway have enhanced ubiquitination in the *upl3* mutant, while those in the inositol-1,4,5-trisphosphate-3-kinase (IP3K) signaling pathway have reduced ubiquitination in the *upl3* plants versus WT (Figure 5D-E), which included 5 proteins, namely ABCG36, MS2, PPC2, LOS1, and AT3G63160 (Figure 5E, fold-change depicted in blue). 14 other interacting candidates showing *upl3*-mutation-enhanced ubiquitination in the *upl3* background were H2AXb, RPS2B, PHOT1, ERD14, the SWI-SNF chromatin remodeling ATPase BRAHMA (BRM) and SWIS3C, as well as carbon-metabolism-related enzymes (Figure 5E, fold-change depicted in orange). Notably, UBP12, UBP13, and UBP26 are also among the UPL3 interacting candidates (Figure 5E). UBP12 is a ubiquitin hydrolase, with a demonstrated de-ubiquitination activity *in vitro* and localization both in the cytoplasm and the nucleus (Deracheva et al., 2016; Kralemann et al., 2020).

The UPL3-interacting and target proteins UBP12 and BRM are involved in leaf development and aging

To confirm these putative UPL3 interacting partners, we carried out a yeast two-hybrid assay by selecting 16 candidates. The self-interacting N-terminal fragment (470 aa) of UPL3 containing armadillo repeats was shown interacting with most of the selected candidates except for UPL5 and PHOT1, however, the full-length UPL3 only showed a strong interaction with BRM and UBP12, and very weak interaction with HXK1, PPC2 and UBC35 (Figure 6A-B), but the full-length UPL3 bait was not able to interact with its N-terminus (Figure 6B). The failure to detect many interactions with the full-length bait may be explained by a degradation effect mediated by the ligase activity retained in the yeast cell, although that needs to be further verified. Next, the interaction of UPL3 with UBP12 was confirmed using BD-UBP12 as a bait, which in turn showed a weak interaction with two other UPL3-interactors, namely the BRM and PPC2 (Figure 6C).

To examine whether UPL3 altered the protein level of the bound candidates of UPL3 between *upl3* and WT. To the end, we compared the total proteomes of 6-week-old wild-type and the *upl3* plants by tandem MS using the precursor ion intensity of the MS1 scans for quantification. Altogether, 3557 Arabidopsis proteins could be reproducibly identified and quantified in both samples by our liquid chromatography-mass spectrometry (LC-MS) regime analyzed in triplicate (Supplementary Fig S8; Supplementary Dataset

S4). We searched for the protein level of UBP members and several interested proteins in differentially expressed proteins (DEPs) of proteome dataset from *upl3*/WT (Supplementary Dataset S4). Several UPL3-bound proteins BRM, UBC35, UBP12, and UPL13, as well as other UBP members such as UBP1C, UBP6, UBP26 were slightly upregulated 1-1.4 folds in the *upl3* mutant relative to WT; the rest UPL3-bound proteins HXK1 and PPC2 exhibited a downregulated 1.5-3 folds in the *upl3* mutant relative to WT (Figure 6D; Supplementary Dataset S4). Furthermore, when the ubiquitination enrichment was normalized to protein level, the level of ubiquitinated UBP12, UBP13, and UBP26 was not significantly changed between the *upl3* and WT, however, the protein level of ubiquitinated BRM, UBC7 and HXK1, PPC2 maintained same up/down altered potential (Figure 6D-E). This suggests that UBP12 and other UBP members are interacting partners but not substrates of UPL3 as E3 ligase.

To examine whether the interaction between UPL3 and UBP12 might contribute to the level of ubiquitinated targets in *planta*, we first detected BRM and PPC2 ubiquitination in *ubp12* and *upl3* mutant background using antibodies against poly-ubiquitin, BRM, and PPC2. The total ubiquitination level in the *ubp12* or the *upl3* was comparable or slightly stronger than in the wildtype, while it declined considerably in the *UBP12*-overexpressing line (Figure 6E). The protein levels of PPC2 were increased by either *upl3* mutation or its overexpression, as well as in *ubp12* mutant, they were in contrast diminished by *UBP12* overexpression (Figure 6E). It suggested that UBP12 affected PPC2 protein level more than UPL3 did, although UPL3 affected PPC2 both ubiquitination enrichment and protein level. However, UBP12 and UPL3 displayed opposite effect on BRM protein level when their genes were mutated. Loss of *UBP12* reduced, but loss of *UPL3* increased, the BRM protein accumulation relative to WT, while overexpression of the two genes had the opposite effect to deletion (Figure 6C). We conclude that UBP12 has a major effect on PPC2 protein degradation, while UPL3 and UBP12 antagonistically affect the BRM protein level. These results suggest a complicated molecular interaction network between UPL3 and these proteins, probably in terms of homeostasis in protein ubiquitination.

We further sought insights from phenotypic analysis of the *upl3-1, ubp12, and brm-em* mutant plants. The results showed that *oeUPL3-24*, *ubp12*, and *brm-em* plants shared a common phenotype of early bolting and flowering, but only a double mutant of *ubp12 ubp13* (with 91% sequence identity at the amino acid level) caused the curled-leaves and premature leaf aging phenotype found in the *brm-em* plants (Figure 7A-B; Supplementary Fig S9). In contrast, *upl3* plants displayed a late-senescence phenotype with delayed flowering-time (more than one week), the effect of UPL3 on plant development contrasted those of both UBP12 and BRM (Figure 7C-D), thereby, a mild curled-leaves phenotype was also observed in aging leaves of the *upl3* plants at a later stage of development (Figure 1A, 7A). It is consistent with previous reports of phenotype of *ubp12* and *brm* mutants (Cui et al., 2013; Park et al., 2019; Xu et al., 2016; Li et al., 2016; Archacki et al., 2017).

Furthermore, the starch content of the mutant plants was monitored to check whether the opposite phenotypes observed in *upl3* and *ubp12* were related to carbon metabolism. The *upl3* mutant showed a decreased starch accumulation compared with WT, while complementation or overexpression of *UPL3* restored the starch content to the WT level (Figure 7E). In contrast, the *ubp12* mutant displayed

significantly stronger starch accumulation than that in WT, while effect of *UBP12* overexpression was similar to that of the *upl3* mutant, with a much lower starch content in the plants (Figure 7E). Therefore, starch accumulation is positively correlated to the early flowering phenotypes associated with mutations in the two antagonistic ubiquitination pathway genes.

Analysis of ubiquitin footprints (K sites).

The H89R substitution in the tagged ubiquitinated assay used here enables the detection of ubiquitination sites (“footprints”) and identified a consensus ubiquitin attachment sequence (Xu et al, 2010). By scanning all generated datasets, we identified 2778 ubiquitinated sites in total (Supplementary dataset S1). Among these, 2359 sites were quantified, 1641 of the 2359 sites were in the *upl3* plants, 414 sites were differentially displayed relative to WT plant with a cut-off log2FC of 1.5.

We identified 110 ubiquitinated modification sites on 77 differentially ubiquitinated proteins in *upl3*/WT (log2FC > 2) (Supplementary dataset S2). Motif analysis around the modified lysine using MEME identified a consensus ubiquitin attachment sequence in 44 of the 110 sites (Figure 8A) that strongly matched the c-K-x-E/D/G ubiquitination motif (where c and x represent a hydrophobic and any amino acid, respectively), which was a prevalent motif in yeast and animal ubiquitinated targets (Xu et al. 2010). However, the remaining 66 sites (60%) were unrelated to this motif, indicating that noncanonical sites were also common. In addition, referring to the GPS-SUMO algorism (Zhao et al., 2014), one or more copies of this consensus sequence were detected in ubiquitinated targets accounting for 74%, 66%, and 59% of the three enriched ubiquitination categories, the UPL3-dependent, abundant, and total ubiquitinated proteins, respectively. Among the 44 sites with a consensus sequence, out of the 110 sites, 14 out of the 21 mapped attachment sites on 18 UPL3-upregulated targets belonged to the canonical c-K-x-E/D/G motif, with the remainder had alternative sequences (Supplementary Dataset S6), including GAPC1, GAPC2、CASA1、NADP-ME2, RuBisCO, AAT1, FBAB, PGK3, MDH1, GLO1, and SHM4 (Figure 8B). Specifically, the ubiquitinated sites identified here for the UPL3-dependent targets, namely ALDH, OASA1, HXK1, and PPC2 were within a non-canonical x-A-K-x- motif or x-K-A-x motif (Figure 8B), due to HXK1 at K77 was previously reported to be ubiquitinated at a site of non-canonical linkages in animal cell (Huang and Li, 2018). Thus, our omics results confirm the assembly of poly-ubiquitin chains in plants. By scanning our ubiquitome datasets for ubiquitination sites using footprints containing ubiquitin remnants after trypsin cleavage, modifications by SUMO1 at K23 and K42 were detected in addition to polyubiquitin linked via K48 linkages. This provides further evidence for SUMOylating of some ubiquitylated proteins in *Arabidopsis* (Miller et al., 2010).

Discussion

During cell senescence, the predominant form of post-translational regulation that has been well-characterized is protein degradation, which is critical not only in signal transduction, but also for the execution of the senescence syndrome (Buchanan-Wollaston, 2005; Woodson, 2015; Yolcu, 2017; Guo et

al., 2021). Our multi-omics analysis provides an overview of UPL3 downstream targets that were either directly or indirectly affected at the protein level and the transcript level. An important and unexpected finding is that loss of UPL3 results in a globally enhanced ubiquitination of metabolism-related proteins and downregulation of expression of a series of senescence related genes (Figure 2, 4). The UPL3-associated ubiquitin conjugates are enriched mostly for proteins involved in molecular interactions (Figure 3), implying a major role of UPL3 in the metabolism-mediated cell senescence regulatory network. The unveiling of physical interactions with the ubiquitin-specific proteases UBP12, the chromatin remodeling ATPase BRM and PPC2 is of particular interest (Figure 5), suggesting potential actin model of UPL3 interacting with UBP12 in chromatin regulation, and metabolic related protein turnover during plant development (Figure 9).

UPL3 alters the levels of ubiquitin conjugates of proteins involved in methionine metabolism, carbon metabolism and heavy metal stress-induced cell senescence

Globally, the loss of the HECT-type E3 ubiquitin ligase UPL3 leads to the depletion of ubiquitin conjugates of specific proteins, accounting for ~ 1/3 of the total proteins whose ubiquitination status is significantly altered, with a ratio > 1.2 (Figure 2). These proteins are considered as putative substrates targeted by the UPL3 enzyme, although not all proven experimentally yet. And some of these are demonstrated UPL3 targets, e.g., GLS3 (Patra et al., 2013; Gao et al., 2017; Saracco et al., 2013; Kim et al., 2015), it did not appear in our dataset, however, other common known ubiquitinated targets included in the list are AHA1, CDC48A, ERD4, LEC2, and RPN proteins (Supplementary Figure S4, and Ref. in Yamauchi et al. 2016; Kumari et al.; 2019; Park et al. 2008, Rai et al. 2012; Finley et al. 2009; Besche et al., 2014; Furniss et al. 2018; Downes et al., 2003), playing roles in cell division, cell senescence, and stress-induced cell senescence.

UPL3 has several additional putative targets, such as MS2 (At3G03780), OASA1 (At4G14880), ALDHA3 (At2g24270), HXK1 (Cho et al. 2006), and PPC2 (AT2G42600). Although direct ubiquitination evidence *in vitro* did not present here, the protein level of these five putative target proteins were accumulated by proteome analysis (Figure 6D; Supplementary Dataset S4) and the ubiquitin level of them were downregulated in the *upl3* mutant relative to WT by ubiquitome analysis (Figure 2, 5; Supplementary Dataset S2); The ubiquitinated sites were identified as a non-canonical pattern (Figure 8); Two of them: HXK1 and PPC2 were detected to be direct interacting partners of UPL3 (Figure 6). This evidence supposed that UPL3 recruited them and might affect their ubiquitin level and protein level in ubiquitination/26S proteasome system (UPS) degradation pathway. It has been reported that these five putative proteins play important roles in promoting cell proliferation and expansion early during leaf development (HXK1, Van Dingenen et al. 2019), delaying flowering and leaf senescence (ALDHA3, Stiti et al. 2011), reducing starch accumulation (PPC2, Shi et al. 2015), and lowering cadmium tolerance, defense response against abiotic stresses such as salicylic acid, salinity, heavy metal, and leaf cell death (OASA1, Shirzadian-Khorramabad et al., 2010; Dominguez-Solis et al., 2001; Birke et al., 2013), which is consistent with the *upl3* phenotype (Figure 1 and Figure 7; Furniss et al., 2018). Among them, it has known that HXK1, can also interact with a senescence/dehydration-associated protein, early responsive

to dehydration 7 (ERD7; AT2G17840), and a histone H2A protein, HTA6 (AT5G59870) in the nucleus. Nuclear HXK1 forms a glucose signaling complex core that regulates cell proliferation and expansion early during leaf development (Van Dingenen et al. 2019); Phosphoenolpyruvate carboxylase (PPC2) is a crucial enzyme that catalyzes an irreversible primary metabolic reaction but might be a reversible amino acid metabolic pathway in C3 plants. PPC1 and PPC2 are highly expressed in *Arabidopsis* leaves (Shi et al. 2015). Both *ppc2* and *ppc1ppc2* exhibited a severe growth-arrest phenotype and accumulated more starch and sucrose than wild-type plants (Shi et al. 2015; You et al., 2020); however, PPC2 protein levels increased in both *upl3* and *oeUPL3* plants, while PPC2 protein levels decreased in the *oeUBP12* plants, which exhibited a decreased starch and sucrose accumulation in *upl3* and *oeUBP12* plants, compared to WT (Figure 6, 7). This inconsistence may be explained that PPC2 might not be a direct target of UPL3 to affect metabolite flux in carbon fixation in C3 plant such as *Arabidopsis*; In most nonphotosynthetic tissues and the photosynthetic tissues of C3 plants, the fundamental function of PEPC is to anaplerotically replenish tricarboxylic acid cycle intermediates, which can be activated by its positive effector, Glc-6-P, and inhibited by its negative effectors, such as malate, Asp, and Glu, as well as the levels of glycine and serine (O'Leary et al., 2011; You et al., 2020). Our result showed that UPL3 also affected the ubiquitin level of MS2 and OASA1 in methionine and cysteine biosynthesis pathway (Figure 3), which perhaps it feedbacks negatively regulates PPC2 protein level through amino acid biosynthetic process. Besides, it is surprising that although a large set of enriched ubiquitinated conjugates in *upl3* plants might not be direct targets of UPL3, they are mostly enriched in the carbon fixation pathway such as ALDO, GAPDH, RBCL, PGK (Figure 3C) by analysis of ubiquitin footprints, which might be affected metabolite flux direction to amino acid metabolism pathway by UPL3-PPC2 regulatory module in carbon fixation. This suggests that UPL3 may form a complex with these five substrates to alter their protein level *via* ubiquitination/26S proteasome system (UPS) degradation pathway, and play roles in methionine and carbon metabolism related cell senescence and plant aging.

UBP12 is an UPL3-interacting protein, which in-turn might act as an important downstream player in protein ubiquitination

As described in previous review, the HECT E3 N-terminus not only simply serves as an adapter for direct binding, but it also provides various ways to regulate HECT E3s' substrate recruitment and catalytic activity (Lan and Miao, 2019). In this study, we showed that UPL3 seemed to interact with histone variants, histone modifiers (BRM), PPC2, several U-box proteins (UBC35) and DUBs (UBP12) in the nucleus (Figure 6). The ubiquitin conjugates were all enhanced in the *upl3* plants (Figure 2). If we only look at canonical function of UPL3 E3 ligase in the UPS pathway, it seems to be hard to explain the UPL3 affecting on polyubiquitination. Furniss et al (2018) suggested that UPL3 might have E4 function, recruiting polyubiquitin to targets (Furniss et al., 2018), however it could not explain our issue yet. This study showed that UPL3 could interact with UBP12, UBP13 and UBP26, as well as BRM, HXK1, and PPC2 (Figure 5, 6), however, the protein level of UBP12, UBP13, UBP26, and other members were not significantly altered. Thus, we supposed that UBP12, UBP13 and UBP26 might be recruited by UPL3 for nuclear access or playing their roles together. In fact, it has reported that UBP12 has function in the protein deubiquitination and is able to interact *in vivo* with a Polycomb G protein (LHP1) and EMBRYONIC

FLOWER1 complex (EMF1c) to form a complex and make removal of H2A ubiquitin, being necessary for correct biological function in plant senescence and flowering and repress genes involved in stimulus response (Li et al., 2018; Kralemann et al., 2020). In this study, similar phenotypes among *oeUPL3*, *ubp12*, *ubp12 ubp13*, and *brm* mutant or between *upl3* and *oeUBP12* are helpful to explain UPL3 and UBP12 playing their roles together to determine ubiquitination status of histone variants or candidate targets for correct biological function in plant senescence and flowering and organ development. *oeUPL3* had more similar phenotype with the *ubp12 ubp13* double mutant: early flowering (An et al., 2018; Cui et al., 2013), premature leaf aging phenotype (Park et al., 2019; Vanhaeren et al., 2020), and response to SA (Furniss et al., 2018) and JA (Ewan et al., 2011; Jeong et al., 2017), as well as plant defense response (Brazma et al., 2003; Ewan et al., 2011), while the *ubp12* mutant showed starch accumulation similar to UPL3-overexpressing plants (Figure1, 7). The interaction of UBP12 with PPC2 led to PPC2 protein degradation (Figure 6E), displaying less starch accumulation similar in the *oeUBP12* plants. Similarly, the interaction of UBP12 with BRM led to BRM protein accumulation in the *oeUBP12* plant; in contrast, BRM protein was accumulated in the *upl3* plant (Figure 6E), exhibiting a delayed senescence and flowering phenotype. Furthermore, a series of transcription factors, such as WRKYs, MYBs, ZFs and NACs are common downstream genes of UPL3 and UBP12/13 (Figure 4; Lee et al., 2019). It is speculated that UPL3 might recruit UBP12/UBP13 in enhancing the de-ubiquitination of a large set of proteins, such as carbon metabolism related enzymes. The detailed insight into the regulatory mechanism between UPL3 and UBP12/13 would be addressed in the future. Furthermore, in this study UPL3 seems to alter H2A or other histone variants ubiquitin level (Figure7, 8), and UBP12/13 were reported to be involved in H2A deubiquitination, which removal of H2Aub1 by UBP12/13 prevents loss of H3K27me3 and repress gene expression (Kralemann et al., 2020). These examples suggest that UPL3 and UBP12/UBP13 modified targets might share functional similarities to other epigenetic mechanisms, and the study of multi-epigenetic modifications in certain loci in a specific cell type during development will be the next challenge in the field.

The UPL3 active site is dependent on the non-canonical ubiquitination motif

Based on the analysis of the Kub site information in this study, the canonical c-K-x-E/G motif sites are highly enriched in the ubiquitin conjugates in the *upl3*, whereas the non-canonical motif –x-A-K-x- sites show low enrichment (Figure 8), although the underlying mechanism is still unclear. According to acetylation of lysine (Kac) sites of GAPDH protein both in human and in rice under stress condition is required for protein translocation into the nucleus (Boukouris et al., 2016; Huang et al., 2018; Li et al., 2016). Our data presented here indicate that one lysine (K76 in AtGAPC) was ubiquitinated in the *upl3* plants. Whether it is necessary for AtGAPC's function is still unclear, However, different extracellular stimuli and their intracellular signaling messengers (e.g., heat, salt, osmotic stress, heavy metal, reactive oxygen species, and lipid mediators) might differentially and specifically induce ubiquitination of GAPC for nuclear access *via* Kub site pattern (Li et al., 2016; Kim et al. 2020). Therefore, we speculate that the Kub site preference pattern of UPL3 mediates their function and regulation.

Materials And Methods

Materials

The seeds of Arabidopsis (*Arabidopsis thaliana*) Col-0 and transgenic plants were germinated, and seedlings were grown on half-strength Murashige–Skoog (MS) medium supplemented with 0.7% (w/v) agar. 10-day-old seedlings were transplanted to the vermiculite, watering with half-strength MS medium in climate rooms under controlled conditions (22.5°C, 13/11 h of light/dark photoperiod with a light intensity of 80 μmol photons m^{-2} s^{-1}, 60% relative humidity). The mutant seeds of *upl3-1* (SALK_015334) and *upl3-3* (SALK_117247) were obtained from the Nottingham Arabidopsis Stock Centre (NASC).

UPL3 over-expression (*oeUPL3*) and complementation plants (*comUPL3*, *pUPL3/upl3*) were constructed by cloning the *UPL3* coding sequence into *pCAMBIA3301* vector using SpeI and SmaI under *ACTIN3* promoter and its own promoter P_{UPL3}, which contains 2kb upstream of the *ATG* start codon) with the primers described in Supplementary Table S1. Arabidopsis transformation was performed by the Floral dip method (Clough and Andrew, 1998). The homozygous *upl3* T-DNA insertion knockout mutants were obtained by genome insertion screening and RNA level screening (Supplementary Fig S1) with the primers described in Supplementary Table S3. The *brm-em*, *ubp12, ubp12ubp13*, and *oeUBP12* seeds were kindly provided by Dr. Keqiang Wu (Taiwan University) and Dr. Wenqiang Tang (Hebei Normal University).

Starch staining

Whole rosettes of 18–21-day *ubp12* and *upl3* transgenic plants were either harvested or covered with black trays at 10 a.m. after 2h. At 10 a.m. of the next day, rosettes of covered plants were harvested. Rosettes were cleared in 80% (v/v) ethanol plus 5% (v/v) formic acid at room temperature, stained in I_2-KI solution (5 g I_2 and 10 g KI per 100 ml sterile water) and washed three times in water (Huang, et al., 2020).

Protein extraction, Trypsin Digestion, HPLC Fractionation, Affinity Enrichment, and LC-MS/MS Analysis

The rosette leaves of ten 6-week-old *upl3* and wildtype plants were pooled and ground in liquid nitrogen into cell powder and then transferred to a 5 mL centrifuge tube, collected in three tubes for one biological replicates, a total of 30 plants were collected for three biological replicates. After that, flowing the method described in Supplementary Method S1.

Database Search

The resulting MS/MS data were processed using the Maxquant search engine (v.1.5.2.8). Tandem mass spectra were searched against the Uniprot database concatenated with a reverse decoy database.

Trypsin/P was specified as cleavage enzyme allowing up to 4 missing cleavages. The mass tolerance for precursor ions was set as 20 ppm in First search and 5 ppm in Main search, and the mass tolerance for fragment ions was set as 0.02 Da. Carbamidomethyl on Cys was specified as fixed modification and GlyGly on Lys and oxidation on Met were specified as variable modifications. Label-free quantification (LFQ) method (Xu et al., 2010) was employed to calculate the relative abundance of the modified peptides, FDR was adjusted to < 1% and minimum score for modified peptides was set to > 40.

Ubiquitin Footprints

Ubiquitin footprints were identified through Proteome Discoverer (version 2.0.0.802; Thermo Fisher Scientific) by searching the TAIR10 protein database using the variable modification of lysine residues by ubiquitin (Gly-Gly, +114.043 m/z). Peptides were assigned using SEQUEST HT (Thermo Fisher Scientific), with search parameters set to assume trypsin digestion with a maximum of two missed cleavages, a minimum peptide length of 6, precursor mass tolerances of 10 ppm, and fragment mass tolerances of 0.02 D. Carbamidomethylation of cysteine was specified as a static modification, while oxidation of methionine and N-terminal acetylation were specified as dynamic modifications. The target FDR of #1% (strict) was used as validation for PSMs and peptides. Proteins that contained similar peptides and which could not be differentiated based on the MS/MS analysis alone were grouped to satisfy the principles of parsimony. MEME Suite 4.11.4 was used to identify the Ubiquitin binding cKxE/D/G motif, whereas the prevalence of these sites was predicted by referring to GPS-ubiquitin (Zhao et al., 2014).

GFP-nanotrap-MS analysis

The rosette leaves of ten 6-week-old *ACTIN3:UPL3-GFP* over-expression plants and *ACTIN3: GFP* plants were harvested and ground in liquid nitrogen and homogenized in immunoprecipitation (IP) buffer (50 mM Tris-HCl pH7.4, 150 mM NaCl, 1 mM EDTA, 1% Nonidet P-40, 1 mM PMSF, 10% Glycerol and 1x Protease inhibitor cocktail (Roche)). After centrifugation at 16000 *g* for 10 min at 4℃, the supernatant of each sample was mixed with 30 µl GBP-beads (Supplementary Fig S6) (Rothbauer et al., 2008) and rotated at 4℃ for 2 hours. GBP-beads were pelleted and washed 5 times with IP buffer. The immunoprecipitated proteins were eluted from the beads with 2x SDS-PAGE sample buffer by heating at 95℃ for 10 min. Triplicate protein samples were separated by 15% SDS-PAGE and then extracted for mass spectrometry analysis according to Deng et al. (2016). Antibody against GFP was purchased from Roche company.

Semi-qRT-PCR and RT-qPCR

Semi-qRT-PCR and RT-qPCR analyses employed the oligonucleotide primers described in Supplementary Table S3 and S4. RNA was extracted from rosette leaves of 6-week-old *upl3* and wildtype plants, the following procedure was performed according to the description (Huang et al., 2020). Semi-qRT-PCR was performed on an ARKTIK thermal cycler (Thermo Scientific). The *GAPC2* (AT1G13440) was chosen as an

internal control (25 cycles). PCR products were run on a 1.0% TAE agarose gel. The transcript abundance of RT-qPCR was normalized to that generated with *GAPC2* based on the comparative threshold method (Pfaffl, 2001). Three independent biological replicates with three technical replicates were performed.

Yeast two hybrid assay

Yeast two-hybrid assays were performed as described in the manual for the GAL4-based two-hybrid system 3 protocol (Clontech). Full-length or different regions of candidates were cloned into pGADT7-AD vectors to construct prey constructs, and the Bait vector pGBKT7-BD expressed the wild type UPL3 or UPL3 variants fused to the GAL4 DNA binding domain (BD). The procedure was according to the described by Huang et al. (2020). The primers were listed in Supplementary Table S2.

Western blot analyses

To extract soluble proteins from plant tissue of *oeUPL3*, *upl3*, *ubp12*, and *oeUBP12* and WT plants, 200 mg of leaf material were batch-frozen in liquid nitrogen, ground into powder, resuspended in 100 µl of extraction buffer (100 mM Tris, pH 7.2, 10% sucrose, 5 mM $MgCl_2$, 5 mM EGTA, protease inhibitor), and centrifuged at 15 000 g for 10 min. The supernatant was used for immunoblotting analysis. Antibodies against polyubiquitin (Agrisera), BRM (kindly provided by Dr Rongcheng Lin, Institute of Botany, Chinese Academy of Sciences), and b-Tubulin (CW0098, KWBIO, China) were used. The procedure was performed according to Miao and Zentgraf (2010). Proteins were separated on 6% acrylamide gels and transferred to nitrocellulose membranes using standard protocols.

Bioinformatic Analysis

Bioinformatic analysis was performed according to previously described protocols (Xie et al., 2015). The detail procedure described in Supplementary Method S2.

All datasets have been deposited to the ProteomeXchange Consortium via the PRIDE partner repository with the dataset identifier PXD027037. The description of dataset was shown in Supplementary Table S5.

Declarations

Acknowledgements

We thank the Nottingham Arabidopsis Stock Centre (NASC) for T-DNA insertion lines. Dr. Rongcheng Lin (Institute of Botany, Chinese Academy of Sciences) kindly provided the antibody against BRM, and Dr. Keqiang Wu (Taiwan University) provided the *brm-em* seeds, Dr Wenqiang Tang (Hebei Normal University) provided the *ubp12*, *ubp12ubp13*, and *oeUBP12* seeds. We thank Jingjie PTM Biolabs for providing the methods for partial data analysis. This work was supported by grant of National Natural Science

Foundation of China (grant number 31770318) and grant of excellent PhD candidate program of Fujian Agriculture and Forestry University. We thank Dr. Binghua Wu (Fujian Agriculture and Forestry University) for critically reading the manuscript.

Conflict of interest

The authors declare no conflicts of interest.

Author Contributions: W.L, S.Z. and H.L. conceived the original screening and research plans including phenotype observation; Y.M. supervised the experiments; W.L. performed protein isolation, starch measurements, yeast two hybrid, and the protein subcellular localization; W.M. performed the immunoblot and ubiquitination assay, Q.Y. and C.H. provided technical assistance to all.; Y.Z and W.L bioinformatics analysis and graphs preparation; Y.M. designed the experiments and analyzed the data; Y.M. conceived the project and wrote the article with contributions of all the authors; Y.M. supervised and completed the writing. Y.M. agrees to serve as the author responsible for contact and ensures communication.

References

1. An Z, **et al** (2018) Regulation of the stability of RGF1 receptor by the ubiquitin-specific proteases UBP12/UBP13 is critical for root meristem maintenance. *Proc Natl Acad Sci U S A*, PMID 29339500,
2. Archacki R, Yatusevich R, Buszewicz D, Krzyczmonik K, Patryn J, Iwanicka-Nowicka R, Biecek P, Wilczynski B, Koblowska M, Jerzmanowski A, **and** Swiezewski S. (2017) Arabidopsis SWI/SNF chromatin remodeling complex binds both promoters and terminators to regulate gene expression. *Nucleic Acids Res.* **45**(6): 3116–3129.
3. BensussanM, Lefebvre V, Ducamp A, Trouverie J, Gineau E, Fortabat MN, Guillebaux A, Baldy A, Naquin D, Herbette S, **et al**. (2015) Suppression of Dwarf and irregular xylem Phenotypes Generates Low-Acetylated Biomass Lines in Arabidopsis. *Plant Physiol.* **168**: 452–463.
4. Berndsen, C.E.; Wolberger, C. (2014) New insights into ubiquitin E3 ligase mechanism. *Nat. Struct. Mol. Boil.* **21**: 301–307.
5. Besche HC, Sha Z, Kukushkin NV, Peth A, Hock EM, Kim W, Gygi S, Gutierrez JA, Liao H, Dick L, **et al**. (2014) Autoubiquitination of the 26S Proteasome on Rpn13 Regulates Breakdown of Ubiquitin Conjugates. *EMBO J.* **33**: 1159–1176.
6. Birke H, Heeg C, Wirtz M, Hell R. (2013) Successful fertilization requires the presence of at least one major O-acetylserine(thiol)lyase for cysteine synthesis in pollen of Arabidopsis. *Plant Physiol.* **163**(**2**):959–72.
7. Buchanan-Wollaston V, Page T, Harrison E, Breeze E, Lim PO, Nam HG, Lin JF, Wu SH, Swidzinski J, Ishizaki K, **and** Leaver CJ. (2005). Comparative transcriptome analysis reveals significant differences

in gene expression and signalling pathways between developmental and dark/starvation-induced senescence in Arabidopsis. *Plant J* **42**: 567–585.

8. Boukouris AE, Zervopoulos SD, Michelakis ED (2016) Metabolic Enzymes Moonlighting in the Nucleus: Metabolic Regulation of Gene Transcription. *Trends Biochem Sci.* **41**(**8**):712–730.
9. Cao Y, Dai Y, Cui S, **and Ma L**. (2008). Histone H2B monoubiquitination in the chromatin of FLOWERING LOCUS C regulates flowering time in Arabidopsis. *Plant Cell* **20**: 2586–2602.
10. Cho YH, Yoo SD, Sheen J. (2006) Regulatory Functions of Nuclear Hexokinase1 Complex in Glucose Signaling. *Cell* **127**:579–589.
11. **Clough SJ** and Bent AF. (1998) Floral dip: a simplified method for Agrobacterium-mediated transformation of Arabidopsis thaliana. *Plant J*, **16**:735–743
12. **Cui X**, Lu F, Li Y, Xue Y, Kang Y, Zhang S, et al. (2013). Ubiquitin-specific proteases UBP12 and UBP13 act in circadian clock and photoperiodic flowering regulation in Arabidopsis. *Plant Physiol.* **162**: 897–906.
13. Debernardi JM, et al. (2014) Post-transcriptional control of GRF transcription factors by microRNA miR396 and GIF co-activator affects leaf size and longevity. *Plant J*, 2014 Aug
14. Deng, X., Lu, T., Wang, L., Gu, L., Sun, J., Kong, X., Liu, C., **and** Cao, X. (2016). Recruitment of the NineTeen Complex to the activated spliceosome requires AtPRMT5. *Proc. Natl. Acad. Sci. USA* **113**: 5447–5452.
15. Derkacheva M, Liu S, Figueiredo D D, Gentry M, Mozgova I, Nanni P, et al. (2016). H2A deubiquitinases UBP12/13 are part of the Arabidopsis polycomb group protein system. *Nat. Plants* **2**:16126.
16. Dominguez-Solís JR, Gutierrez-Alcalá G, Vega JM, Romero LC, Gotor C. (2001) The cytosolic O-acetylserine(thiol)lyase gene is regulated by heavy metals and can function in cadmium tolerance. *J Biol Chem*, PMID 11121418.
17. **Downes**, **BP**, Stupar RM, Gingerich D.J.; Vierstra, R.D. (2003). The HECT ubiquitin-protein ligase (UPL) family in Arabidopsis: UPL3 has a specific role in trichome development. *Plant J.* **35**: 729–742.
18. **Ewan R**, Pangestuti R, Thornber S, Craig A, Carr C, O'Donnell L, et al. (2011). Deubiquitinating enzymes AtUBP12 and AtUBP13 and their tobacco homologue NtUBP12 are negative regulators of plant immunity. *New Phytol.* **191**: 92–106.
19. Finley D. (2009). Recognition and processing of ubiquitin-protein conjugates by the proteasome. *Annu. Rev. Biochem.* **78**: 477–513.
20. **Furniss JJ**, Grey H, Wang Z, Nomoto M, Jackson L, Tada Y, Spoel SH. (2018) Proteasome-associated HECT-type ubiquitin ligase activity is required for plant immunity. *PLoS Pathog.* **14**: e1007447.
21. Gao C, Li D, Jin C, Duan S, Qi S, Liu K, Wang H, Ma H, Hai J, Chen M **(**2017**)**. Genome-wide identification of GLABRA3 downstream genes for anthocyanin biosynthesis and trichome formation in Arabidopsis. *Biochem Biophys Res Commun.* **485**(2):360–365.

22. Guo P, Li Z, Huang P, Li B, Fang S, Chu J, **et al**. (2017) A tripartite amplification loop involving the transcription factor WRKY75, salicylic acid, and reactive oxygen species accelerates leaf senescence. *Plant Cell.* **29**:2854–70.
23. Guo Y, Ren G, Zhang K, Li Z, Miao Y, **and** Guo H. (2021). Leaf Senescence: Progression, Regulation, and Application. *Molecular Horticulture* **1**:5. https://doi.org /10.1186/ s43897-021-00006-9.
24. Huang C, Yu J, Cai Q, Chen Y, Li Y, Ren Y, Miao Y. (2020). Triple-localized WHIRLY2 Influences Leaf Senescence and Silique Development via Carbon Allocation. *Plant Physiol*, 184:1348–1362.
25. Huang H, Tang S, Ji M, Tang Z, Shimada M, Liu X, Qi S, Locasale JW, Roeder RG, Zhao Y, **and** Li X. (2018) p300-Mediated Lysine 2-Hydroxyisobutyrylation Regulates Glycolysis. *Mol Cell* **70**(**4**): 663–678.e6
26. Jeong J S, Jung C, Seo J S, Kim J-K, **and** Chua N-H. (2017). The deubiquitinating enzymes UBP12 and UBP13 positively regulate MYC2 levels in jasmonate responses. *Plant Cell* **29**: 1406–1424.
27. Kanehisa M, Goto S (2000). KEGG: Kyoto Encyclopedia of Genes and Genomes. *Nucleic Acids Res* **28**: 27–30
28. Kim SC, Guo L and Wang X. (2020) Nuclear moonlighting of cytosolic glyceraldehyde-3-phosphate dehydrogenase regulates Arabidopsis response to heat stress. *Nat Commun.* **11**: 3439.
29. Kim J Y, Oh J E, Noh Y S, **and Noh B**. (2015). Epigenetic control of juvenileto- adult phase transition by the Arabidopsis SAGA-like complex. *Plant J.* **83**: 537–545.
30. Kotliński M, Knizewski L, Muszewska A, Rutowicz K, Lirski M, Schmidt A, Baroux C, Ginalski K, **and** Jerzmanowski A. (2017) Phylogeny-Based Systematization of Arabidopsis Proteins with Histone H1 Globular Domain1. *Plant Physiol*. **174**(1): 27–34.
31. Kralemann L, Liu S, Trejo-Arellano MS, Munoz-Viana R, Koehler C, **and** Hennig L. (2020) Removal of H2Aub1 by ubiquitin-specific proteases 12 and 13 is required for stable Polycomb-mediated gene repression in Arabidopsis. *Genome Biol.* **21**: 144.
32. Kumari A, Chetelat A, Nguyen CT, Farmer EE. (2019) Arabidopsis H+-ATPase AHA1 controls slow wave potential duration and wound-response Jasmonate pathway activation. *Proc. Natl. Acad. Sci. USA* **116**(40):20226 -20231
33. Lan W and Miao Y. (2019) New Aspects of HECT-E3 Ligases in Cell Senescence and Cell Death of Plants. *Plants*, **8**: 483.
34. Lee CM, Li MW, Feke A, Liu W, Saffer AM and Gendron JM. (2019) GIGANTEA recruits the UBP12 and UBP13 deubiquitylases to regulate accumulation of the ZTL photoreceptor complex. NATURE COMMUNICATIONS, 10:3750.
35. Li L. et al. (2016). SIRT7 is a histone desuccinylase that functionally links to chromatin compaction and genome stability. *Nat Commun* **7**: 12235.
36. Li C, Gu L, Gao L, Chen C, Wei CQ, Qiu Q, Chien CW, Wang S,Jiang L, Ai LF, Chen CY, Yang S, Nguyen V, Qi Y, Snyder MP, Burlingame AL, Kohalmi SE, Huang S, Cao X, Wang ZY, Wu K, Chen X, Cui Y. (2016) Concerted genomic targeting of H3K27 demethylase REF6 and chromatin-remodeling ATPase BRM in Arabidopsis. *Nat Genet.* **48**(6):687–93.

37. Merai Z, Chumak N, Garcia-Aguilar M, Hsieh TF, Nishimura T, Schoft VK, Bindics J, Slusarz L, Arnoux S, Opravil S, Mechtler K, Zilberman, Fischer RL, Tamaru H. (2014). The AAA-ATPase molecular chaperone Cdc48/p97 disassembles sumoylated centromeres, decondenses heterochromatin, and activates ribosomal RNA genes. *Proc. Natl. Acad. Sci. USA* **111**(45):16166-16171.
38. Miao Y, Zentgraf U. (2010). A HECT E3 ubiquitin ligase negatively regulates Arabidopsis leaf senescence through degradation of the transcription factor WRKY53. *Plant J.* **63**: 179–188.
39. Miao Y, **and** Zentgraf U. (2007). The Antagonist Function of Arabidopsis WRKY53 and ESR/ESP in Leaf Senescence Is Modulated by the Jasmonic and Salicylic Acid Equilibrium. *Plant Cell*, **19**: 819–830
40. Miller MJ, Barrett-Wilt GA, Hua Z, **and** Vierstra RD. (2010). Proteomic analyses identify a diverse array of nuclear processes affected by small ubiquitin-like modifier conjugation in Arabidopsis. *Proc. Natl. Acad. Sci. USA* **107**: 16512–16517.
41. Miller C, Wells R, McKenzie **N**,; Trick M, Ball J, Fatihi A., Dubreucq B, Chardot T, Lepiniec L, Bevan MW. (2019). Variation in expression of the HECT E3 ligase UPL3 modulates LEC2 levels, seed size and crop yield in *Brassica napus*. *Plant Cell* **31**: 2370–2385.
42. O'Leary B, Park J, Plaxton WC. (2011) The remarkable diversity of plant PEPC (phosphoenolpyruvate carboxylase): recent insights into the physiological functions and post-translational controls of non-photosynthetic PEPCs. *Biochem J.* **436**(1):15–34
43. Park S, Rancour DM, Bednarek SY. (2008) In Planta Analysis of the Cell Cycle-Dependent Localization of AtCDC48A and Its Critical Roles in Cell Division, Expansion, and Differentiation. *Plant Physiol*, **148**: 246–258
44. Patra B, Pattanaik S, Yuan L. (2013). Ubiquitin protein ligase 3 mediates the proteasomal degradation of GLABROUS 3 and ENHANCER OF GLABROUS 3, regulators of trichome development and flavonoid biosynthesis in Arabidopsis. *Plant J.* **74**: 435–447.
45. Park SH, Jeong JS, Seo JS, Park BS, **and** Chua NH. (2019) Arabidopsis ubiquitin-specific proteases UBP12 and UBP13 shape ORE1 levels during leaf senescence induced by nitrogen deficiency. *New Phytol*, **223**(3):1447–1460.
46. **Pfaffl MW.** (2001). A new mathematical model for relative quantification in real-time RT-PCR. *Nucleic Acids Res.* **29**: e45.
47. Rai A, Suprasanna P, D'Souza SF, Kumar V. **(**2012**)**. Membrane Topology and Predicted RNA-Binding Function of the 'Early Responsive to Dehydration (ERD4)' Plant Protein. *PLoS ONE* **7**(3): e32658.
48. Rothbauer U, **et al**. (2008). A versatile nanotrap for biochemical and functional studies with fluorescent fusion proteins. *Mol Cell Proteomics* **7**(2)::282–289.
49. Rutowicz K, Lirski M, Mermaz B, Teano G, JSchubert J, Mestiri I, Kroteń MA, Fabrice TN, Fritz S, Grob S, Ringli C, Cherkezyan L, Barneche F, Jerzmanowski A, Baroux C. (2019). Linker histones are fine-scale chromatin architects modulating developmental decisions in Arabidopsis *Genome Biol.* **20**(1):157.

50. Saracco SA, Hansson M, Scalf M, Walker JM, Smith LM, **and** Vierstra R. (2009) Tandem affinity purification and mass spectrometric analysis of ubiquitylated proteins in Arabidopsis. *Plant J.* **59**(2):344–358.
51. Shannon P, Markiel A, Ozier O, Baliga NS, Wang JT, Ramage D, Amin N, Schwikowski B, **and** Ideker T. (2003). Cytoscape: a software environment for integrated models of biomolecular interaction networks. *Genome Res.* **13**: 2498–2504.
52. Shi JH, Yi K, Liu Y, Xie L, Zhou Z, Chen Y, Hu Z, Zheng T, Liu R, Chen Y, **and** Chen J. (2015) Phosphoenolpyruvate Carboxylase in Arabidopsis Leaves Plays a Crucial Role in Carbon and Nitrogen Metabolism. *Plant Physiol* **167**:671–681
53. Shirzadian-Khorramabad R, Jing HC, Everts GE, Schippers JHM, Hille J, Dijkwel PP. (2010) A mutation in the cytosolic O-acetylserine (thiol) lyase induces a genome-dependent early leaf death phenotype in Arabidopsis. *BMC Plant Biol*, PMID 20429919.
54. Stiti N, Missihoun TD, Kotchoni SO, Kirch HH, Bartels D. (2011) Aldehydede hydrogenases in Arabidopsis thaliana: biochemical requirements, metabolic pathways, andf unctional analysis. *Frontiers in Plant Science*, **2**(65):1–11
55. Tanaka T, Ikeda A, Shiojiri K, Ozawa R, Shiki K, Nagai-Kunihiro N, Fujita K, Sugimoto K, Yamato KT, Dohra H, Ohnishi T, Koeduka T, Matsui K. (2018) Identification of a Hexenal Reductase That Modulates the Composition of Green Leaf Volatiles. *Plant Physiol* **178**(2):552–564
56. Tsuwamoto R and Harada T. (2011) The Arabidopsis CORI3 promoter contains two cis-acting regulatory regions required for transcriptional activity in companion cells. *Plant Cell Rep* **30**(9):1723–33
57. **Van** Dingenen J, Vermeersch M ·De Milde L, Hulsmans S, ·De Winne N, **Van** Leene J, Gonzalez N, **Dhondt S ·De Jaeger G**, **Rolland F**, **Inzé D**. (2019). The role of HEXOKINASE1 in Arabidopsis leaf growth. *Plant Mol Biol*, **99**:79-93
58. Vanhaeren H, ChenY, Vermeersch M, Milde LD, Vleeschhauwer VD, Natran A, Persiau G, Eeckhout D, Jaeger GD, Gevaert K, Inze D. (2020) UBP12 and UBP13 negatively regulate the activity of the ubiquitin-dependent peptidases DA1, DAR1 and DAR2. eLife 9:e52276.
59. Vierstra R D. (2009). The ubiquitin–26S proteasome system at the nexus of plant biology. *Nat. Rev. Mol. Cell Biol.* **10**: 385–397.
60. Winter D, Vinegar B, Nahal H, Ammar R, Wilson GV, Provart NJ. (2007). An "Electronic Fluorescent Pictograph" Browser for Exploring and Analyzing Large-Scale Biological Data Sets. *PLoS ONE* **2**(8): e718
61. Woodson JD, Joens MS, Sinson AB, Gilkerson J, Salom PA, Weigel D, **Fitzpatrick JA**, **and Chory J**. (2015). Ubiquitin facilitates a quality-control pathway that removes damaged chloroplasts. *Science* **350**: 450-454.
62. Wu G, Cameron JN, Ljung K, Spalding EP. (2010). A role for ABCB19-mediated polar auxin transport in seedling photomorphogenesis mediated by cryptochrome 1 and phytochrome B. *Plant J*, **62**(2):179–91.

63. Xie X, Kang H, Liu W, Wang GL. (2015) Comprehensive profiling of the rice ubiquitome reveals the significance of lysine ubiquitination in young leaves. *J Proteome Res* **14**: 2017–2025
64. Xu G, Paige J and Jaffrey S. (2010). Global analysis of lysine ubiquitination by ubiquitin remnant immunoaffinity profiling. *Nature Biotechnology*, **28** (8):868–872
65. Xu Y, Guo C, Zhou B, Li C, Wang H, Zheng B, Ding H, Zhu Z, Peragine A, Cui Y, Poethig S, Wu G. (2016) Regulation of Vegetative Phase Change by SWI2/SNF2 Chromatin Remodeling ATPase BRAHMA. *Plant Physiol.* **172**(4):2416–2428
66. Yamauchi S, Takemiya A, Sakamoto T, Kurata T, Tsutsumi T, Kinoshita T, Shimazaki K. (2016) The Plasma Membrane H+-ATPase AHA1 Plays a Major Role in Stomatal Opening in Response to Blue Light. *Plant Physiol*, **171**:2731–2743
67. Yang H, Richter GL, Wang X, Młodzińska E, Carraro N, Ma G, Jenness M, Chao D, Peer WA, Murphy AS. (2013) Sterols and sphingolipids differentially function in trafficking of the Arabidopsis ABCB19 auxin transporter. *Plant J*, **74**(1):37-47. d
68. Yang Y, Zhang Y, Ding P, Johnson K, Li X, Zhang Y. (2012) The ankyrin-repeat transmembrane protein BDA1 functions downstream of the receptor-like protein SNC2 to regulate plant immunity. *Plant Physiol* **159**(4):1857–65.
69. Yolcu S, Li X, Li S, **and** Kim YJ. (2017). Beyond the genetic code in leaf senescence. *Journal of Experimental Botany* **69**: 801–810
70. You L, Zhang J, Long Li L, Xiao C, Feng X, Chen S, Guo L, Hu H. (2020) Involvement of abscisic acid, ABI5, and PPC2 in plant acclimation to low CO2. *J Exp Bot.* **71**(14):4093–4108
71. Zhang S, Li C, Wang R, Chen Y, Shu S, Huang R, Zhang D, Li J, Xiao S, Yao N, **and** Yang C. (2017) The Arabidopsis Mitochondrial Protease FtSH4 Is Involved in Leaf Senescence via Regulation of WRKY-Dependent Salicylic Acid Accumulation and Signaling. *Plant Physiol*, 173, 2294–2307.
72. Zhao Q, Xie Y, Zheng Y, Jiang S, Liu W, Mu W, Liu Z, Zhao Y, Xue Y, **and RenJ**. (2014). GPS-SUMO: a tool for the prediction of sumoylation sites and SUMO-interaction motifs. *Nucleic Acids Res*. **42**: W325–W330.
73. Zheng N and Shabek N. (2017). Ubiquitin ligases: structure, function, and regulation. *Annu. Rev. Biochem.* **86**: 129–157.

Supporting Information

Supplementary Fig S1-9, Table S1-5

Supplementary Fig S1 Transcript levels of *UPL3* genes in the *upl3* mutants detected by RT-qPCR

Supplementary Fig2 Expression pattern of UPL3 in various organ and tissue by GUS staining of *Pupl3:GUS line*

Supplementary Fig S3 Quality control of the determination of tryptic peptides of ubiquitin conjugated proteins from 6-week-old *upl3* mutant and wildtype plants

Supplementary Figure S4 List of the UPL3-dependent ubiquitin-enriched (A) and ubiquitin-reduced targets (B) based on *upl3*/WT comparison.

Supplementary Fig S5 Protein domain analysis of DUCs with significant fold-change.

Supplementary Fig S6 Gene Ontology (GO) Enrichment of the differentially regulated ubiquitin conjugates (DUCs) of *upl3*/WT by Cytoscape.

Supplementary Fig S7 Preparation and quality detection of GFP binding protein bead

Supplementary Fig S8 Proteomic analysis of 6-week-old *upl3* mutant and wildtype plants

Supplementary Fig S9 Phenotyping of *ubp12ubp13* mutant

Supplementary Table S1-4 List of primer sequences in this study

Supplementary Table S5 The description of datasets

Supplementary Dataset S1-6

Figures

Figure 1

Phenotype of representative 6-week-old wild-type and *upl3* plants.

A. Organization of the *UPL3* gene and plasmid constructs for transgenic plants.

B. Immunodetection of UPL3-GFP protein in the *upl3* (*upl3-1*, *upl3-3*), complemented line (pUPL3/*upl3-1*) and oeUPL3 transgenic plants (*oe-24*, *oeUPL3-24*; *oe-39*, *oeUPL3-39*), with an antibody against GFP. The GFP control is from transgenic plants expressing the GFP alone. Red arrowhead indicates UPL3-GFP (250kDa).

C. Phenotype of representative 6-week-old wild-type, *upl3-1*, and *oeUPL3*-24 transgenic plants. Leaf senescence and curled leaves are indicated.

D. Chlorophyll content and carotenoid content measured in the rosettes of 6-week-old wild-type, *upl3-1*, and *oeUPL3-24* plants. Chla, chlorophyll a; Chlb, chlorophyll b; ChlT, total chlorophyll; Cxc, carotenoid.

E. Photosystem II fluorescence activity (Fv/Fm) of rosette leaves of 6-week-old plants (n=9).

F. Proportion of green and yellow leaves of whole rosette of 8-week-old plants (n=12).

Error bars represent the standard deviation of six biological replicates. Asterisks denote statistically significant differences from the WT, calculated using Student's t test: *, P<0.05; **, P < 0.01; and ***, P< 0.001.

G. Flowering time of the wild-type, *upl3-1*, and *oeUPL3-24* plants (n > 20). Percent flowering indicated ratio of flowering plants and no flowering plants

H. Representative images showing the bolting of plants in the 7th week after germination.

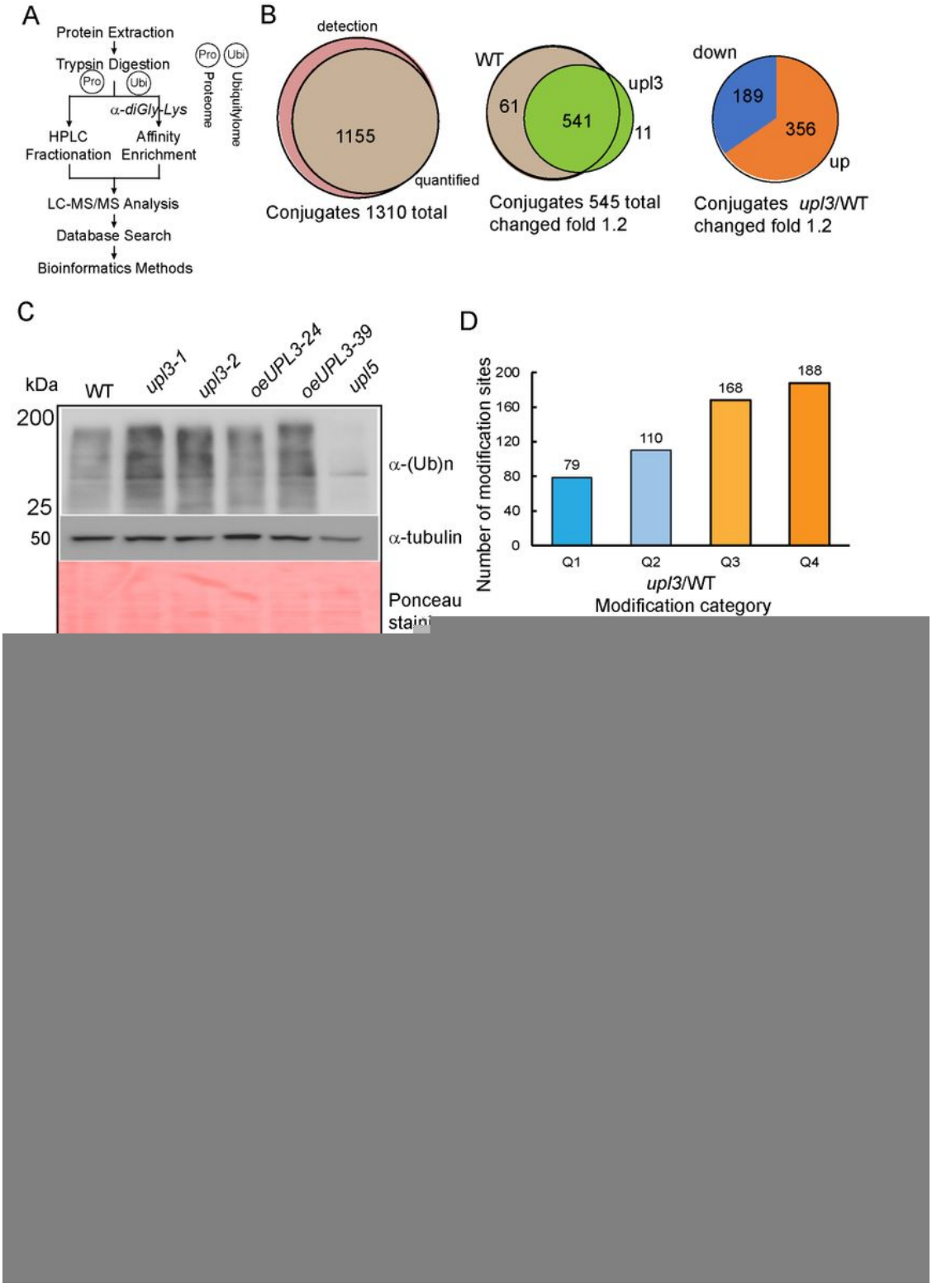

Figure 2

Identification of ubiquitin conjugates in 6-week-old *upl3* plants compared to wild-type

A. A label-free mass spectrometry-based analysis procedure of protein ubiquitination using K-epsilon-GG remnant antibody enrichment approach.

B. Venn diagrams showing the enrichment of differentially ubiquitinated proteins in the *upl3* background.

C. Immunodetection of global ubiquitinated proteins in plants of WT and mutants using antibody against ubiquitin. The *upl5* plant is included for a comparison. WB of b tubulin and membrane ponceau staining are used as protein loading controls.

D. Distribution of enriched proteins within differential fold-change levels by *upl3* relative to WT

E. Volcano plot of individual ubiquitination site showing their P value and the log2 FC. Dark-gray points are conjugates considered to be “abundant” by their detection in three biological replicates in either background (*upl3* and/or the wild type). Proteins with a significant decrease or increase in ubiquitination in the *upl3* mutant compared with the wild type (P value< 0.05) are highlighted in red and blue, respectively. Ubiquitinated targets identified in all wild-type biological replicates and never or only once in the *upl3* mutant, but that were above the significance threshold of P value > 0.05, are in yellow. The dashed line represents the theoretical situation, where conjugate abundance in the wild type and *upl3* is equal. The horizontal dashed line highlights a P value = 0.05. The vertical dashed lines highlight a 1.2-fold (log2 FC = 0.26) increase or decrease.

Figure 3

GO term and KEGG pathway enrichments for the UPL3-associated ubiquitin conjugates

A. GO term enrichment in categories of molecular functions.

B. Bubble plots showing KEGG pathway of enriched DUCs.

C. The UPL3-influenced ubiquitin conjugates of the *upl3*/WT mapped in carbon fixation pathway

D. The UPL3-dependent ubiquitin conjugates of the *upl3*/WT mapped in cysteine and methionine metabolism pathway

E. Distribution of UPL3-influenced DUCs associated with cellular components.

F. Subcellular localization of UPL3 in the nucleus of *Arabidopsis* leaves transiently expressing a C-terminal GFP fusion. The GFP-alone expressing leaves sample is used as control. The nucleus is counter-stained with DAPI.

Figure 4

Co-analysis of UPL3-dependent transcriptome highlights stress-related genes.

A. Enriched protein domains of DUCs *via* InterProScan

B. Venn diagrams showing overlaps of DUCs (fold change > 1.5) and transcriptome DEGs (log2FC > 1.3) of *upl3* relative to WT, RNA-seq data released from the ArrayExpress database at EMBL-EBI (www.ebi.ac.uk/arrayexpress) under accession number E-MTAB-7374 (Furniss et al., 2018).

C. GO terms enrichment analysis of 1467 differential display genes (DEGs) of *upl3*/WT

D. Quantitative real-time PCR of gene expression from 6-week-old *upl3* and wildtype plants for 14 selected plant aging and senescence related transcription factors. Error bars represent the standard deviation of three biological replicates.

E. List of the 26 overlapping genes of DUCs and DEGs, as in B. Text in blue and orange denotes a down or up regulation in the *upl3* plants, respectively.

Figure 5

UPL3-interacting proteins overlapping with DUCs identify potential UPL3-ubiquitinated substrates ABCG36, MS2, OEP6, PPC2 and LOS1

A. Immunodetection of protein samples isolated from GFP and UPL3-GFP-expressing plants with an antibody against GFP.

B. Nano-trapped proteins for MS analysis.

C. Overlapping proteins between UPL3-interacting candidates and the DUCs. 81 putative interacting proteins were identified as specific to UPL3-GFP, which contained 29 and 11 DUCs with a fold-change of 1.2 and 1.5, respectively.

D. Enrichment of KEGG pathway in the overlapping genes highlights an involvement of potential UPL3-ubiquitinated substrates in IP3K pathway and in ribosomal activity.

E. List of most notable interacting candidates of UPL3 with their respective fold ratio of ubiquitination level in *upl3* versus wild-type plants.

Figure 6

Confirmation and characterization of UPL3 interaction with its targets

A. Domain structure of the UPL3 protein showing the full-length and the N-terminus used in Y2H assay.

B Confirmation of UPL3 interaction with its targets in a yeast two hybrid assay. AD or BD empty vector was used as negative control, interacting pair UPL5-WRKY53 was used as a positive control. SD/-LT: SD media minus Leu and Trp, SD/-ALTH: SD media minus Ade, Leu, Trp, and His.

C. UBP12 interacts with BRM, PPC2 but not HXK1 in a yeast two hybrid assay. SD/-LT: SD media minus Leu and Trp, SD/-LTH: SD media minus Leu, Trp, and His, SD/-ALTH: SD media minus Ade, Leu, Trp, and His.

D. The fold-changes of UBP proteins and BRM, PPC1, PPC2, UBC2, UBC7, HXK1 from proteome dataset of *upl3*/WT (Supplementary Dataset S4)

E. Immuno-detection of ubiquitin conjugates (representation: BRM and PPC2) in the *upl3* and *ubp12,* overexpression UPL3 and UBP12 plants compared to wildtype plants. Antibodies against BRM (provided by Dr. Rongcheng Lin), PPC2 (Agrisera) and poly-ubiquitin (Cell Signaling Tech) are used, the b tubulin level and membrane ponceau staining are used as protein loading controls.

Figure 7

The *brm-em*, *ubp12,* and oe*UPL3* plants show similar early leaf senescence and early flowering phenotypes

A. Phenotypes of 5-week-old plants.

B. Bolting and flowering phenotype of the 5-week-old plants.

C. Percent flowering plants of different genotypes at indicated time (n > 20).

D. Chlorophyll content in rosette leaves of 6-week-old plants (n = 3).

E. Photosystem II fluorescence activity (Fv/Fm) of rosette leaves of 6-week-old plants (n=5)

F. Proportion of green and yellow leaves of whole rosette of 8-week-old plants (n=12).

G. Starch staining with KI and quantification in 18-21-day-old rosettes (n=5).

Error bar represents the SD of triplicates. Asterisks denote statistically significant level different with the wild type, as verified via Student's t test: *P, 0.05; **P, 0.01, n =5.

Figure 8

Motif analysis of ubiquitinated protein sites.

A. The consensus ubiquitin attachment motif identified by the MEME Suite.

B. List of apparent ubiquitin attachment sites and motif in identified proteins (fold change >1.5). R1 and R2 are two replicates. Those upregulated and downregulated in *upl3* relative to WT were highlighted in red and blue, respectively.

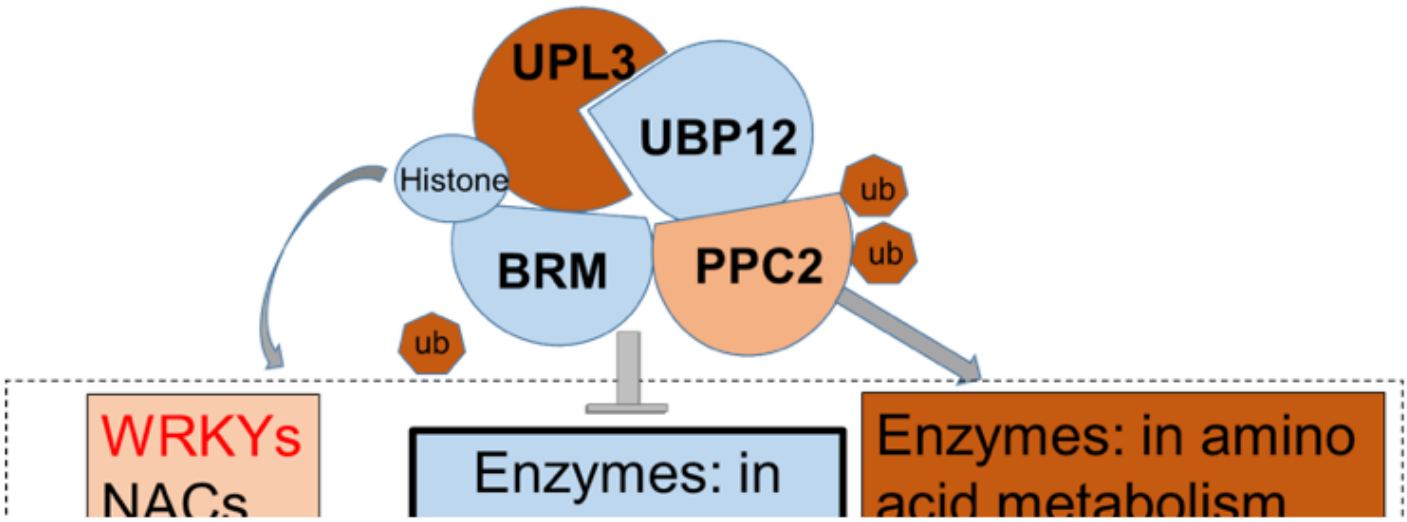

Figure 9

A non-canonical working model of UPL3 in regulating cell senescence of *Arabidopsis* by multi-omics and genetics analysis.

Based on intergrative datasets of ubiquitome, proteome, and transcriptome. Preferential ubiquitination of proteins related to carbon fixation represented the largest set of proteins with increased ubiquitination in the *upl3* plant, while a small set of proteins with reduced ubiquitination caused by the *upl3* mutation were linked to cysteine/methionine synthesis processes. Notably, ubiquitin hydrolase 12 (UBP12), BRM, and PPC2 were among the UPL3-interacting partners identified as the UPL3-interacting partners by both GFP-nanotrap-Mass-Spectrometry analyses and yeast two-hybrid assay; Characterization of *upl3*, *brm-em*, *ubp12*, and *ubp12ubp13* double mutant plants and transcriptome analysis suggested that UPL3 fine-tunes carbon metabolism mediating cellular senescence *via* proteolysis-independent regulation and proteolysis-dependent degradation on metabolism mediated cell senescence. Red color presents upregulated, blue color presents down regulated, thick frame presents more numbers of ubiquitinated proteins

Supplementary Files

This is a list of supplementary files associated with this preprint. Click to download.

- SupplementaryDatasetS1.xlsx
- SupplementarydatasetS2fold2DUTsofupl3wt.xlsx
- SupplementarydatasetS3DEGofupl3wt.xlsx
- SupplementaryDatasetS4DEPofupl3wt.xlsx
- SupplementarydatasetS5DBPofupl3WT.xlsx
- SupplementarydatasetS6Motifanalysis.xlsx
- CRSupplementaryFig19TableS15MethodS12.pdf